East African Journal of Biophysical and Computational Sciences
ISSN (Online): 2789-3618 and ISSN (Print): 2789-360X

Journal Information

Volume 6(2), 2025
DOI: https://dx.doi.org/10.4314/eajbcs.v6i2.1S

Homepage:
https://journals.hu.edu.et/hu-journals/index.php/eajbcs

Article History
Received: 15 October, 2025
Accepted: 20 November, 2025
Published Online: 25 December, 2025

How to cite
Bekele S.S. and Arara A.A. (2025). Mathematical Modeling of Smooth Curve from Sampled Data via the Discrete Biharmonic Equation. *East African Journal of Biophysical and Computational Sciences* Volume 6(2), 2025. .1-13

Open Access

ARTICLE

Mathematical Modeling of Smooth Curve from Sampled Data via the Discrete Biharmonic Equation

Samson Seifu Bekele[1,*], **Alemayehu Adugna Arara**[1]

[1]Department of Mathematics, Hawassa University, Ethiopia.
*Corresponding author: samsonse@hu.edu.et

Abstract

Curve reconstruction is the process of estimating a smooth function or curve that fits a given set of data points, either exactly (interpolation) or approximately (fitting). Classical approaches, including global polynomial interpolation, splines, Hermite interpolation, and radial basis function fitting, face challenges when data are sparse, irregularly distributed, or noisy. In this paper, we propose a curve reconstruction method based on the discrete form of the biharmonic equation. The method formulates reconstruction as a constrained quadratic optimization problem, incorporating both equality and inequality constraints and producing globally C^1 smooth curves. The approach is physically interpretable, penalizing excessive bending, as in the case of a thin elastic beam, and can be extended to higher-dimensional surface reconstruction. Performance is evaluated through numerical experiments on known functions and synthetic data with various distributions and constraints, including small perturbation tests to assess stability and robustness. The results demonstrate that the proposed method reproduces the data, enforces the prescribed bounds, and remains stable under irregular sampling and noise.

Keywords: Curve reconstruction; Biharmonic equation; Constrained quadratic programming problem; Interpolation; Variational form.

East African Journal of Biophysical and Computational Sciences (EAJBCS) is already indexed on known databases like AJOL, DOAJ, CABI ABSTRACTS and FAO AGRIS.

1 Introduction

Curve reconstruction is a process by which a curve or function is determined that either fits or passes exactly through a given set of data points. It can be seen as an inverse problem, where the given data are considered as observations and the curve is unknown or is to be estimated. In general, there are two approaches to curve reconstruction, namely interpolation and fitting (approximation, regression). Interpolation is the process of constructing a curve that passes exactly through all given data points. It is suitable when the data are exact. Fitting, on the other hand, involves finding a curve that approximates the data points but may not pass through any of them, often minimizing the total error between the curve and the points. It is appropriate when the data have measurement errors, noise, or uncertainty.

Both approaches are applicable in a number of areas ranging from digital signal processing and numerical integration to computer graphics, computer-aided design (CAD), and geosciences, among others (Farin, 2002; Li & Heap, 2008; Mazarguil et al., 2022; Phillips, 2003; Piegl & Tiller, 2012).

Among the classical interpolation methods, global polynomial interpolation is one, where a unique polynomial of degree n

is chosen to pass through $n + 1$ given data points. This method provides an explicit analytic form for the interpolant. The unknowns in the polynomial are computed by solving a corresponding system of linear equations whose coefficient matrix is a Vandermonde matrix. The method provides a smooth interpolating curve but has some drawbacks. If one data point is added or removed, the polynomial must be recomputed from scratch. Moreover, the coefficient matrix is highly ill-conditioned even for a small number of data points n (e.g., $n \geq 10$ or so), leading to large numerical errors. Lagrange interpolation reformulates the problem using basis polynomials instead of monomials. This formulation provides an explicit, closed-form solution, thereby avoiding the need to solve a system of linear equations. However, it still shares the same core limitation: adding new data requires recalculating the entire polynomial, which makes it computationally expensive (Hoffman & Frankel, 2018; Zarowski, 2004). Newton's divided difference method, on the other hand, improves this by offering a hierarchical recursive form, which reuses previous computations when new points are introduced, making it more practical, though still susceptible to oscillations (Runge's phenomenon) for high degrees (Hoffman & Frankel, 2018; Phillips, 2003).

Instead of relying on a single high-order global polynomial, piecewise polynomial interpolation is an alternative approach that provides a more stable result and avoids some of the aforementioned drawbacks. The simplest examples are piecewise constant (nearest-neighbor) and piecewise linear methods. These methods are easy to implement but are either discontinuous (in the constant case) or only C^0 continuous with sharp corners (in the linear case) at the data points. Spline interpolation generalizes this idea by connecting together low-degree polynomials while enforcing smoothness at the points. In particular, cubic splines ensure the continuity of the function and its first two derivatives. A key property is that, among all globally C^2 interpolants, the natural cubic spline uniquely minimizes the L^2 norm of the second derivative. Different forms exist, such as natural splines, with zero curvature at the ends, and clamped splines, with prescribed endpoint slopes (de Boor, 2001; Schumaker, 2007). Additional approaches for reconstruction using function values can be found in (Farin, 2002; Hoffman & Frankel, 2018).

In addition to interpolation using function values, derivative information can also be incorporated. This is the principle behind Hermite interpolation, which constructs a piecewise polynomial that not only matches the given values but also respects the slopes at each node (Xu & Xu, 2022).

In spatial statistics, kriging is one of the most widely used interpolation methods. It provides the best linear unbiased estimator (BLUE) of unknown values (Chiles & Delfiner, 2012; Journel & Huijbregts, 1978). The method treats the data as realizations of a random field characterized by a covariance function $C(h)$. Predictions at unsampled locations are obtained as weighted averages of observed data, with the weights chosen to minimize the mean square prediction error. As a result, kriging yields unbiased estimates, explicitly accounts for spatial correlation, and quantifies prediction uncertainty. These features make it particularly effective when data are noisy or sparse, although it is not primarily intended for geometric curve reconstruction (Cressie, 1993).

Fitting methods relax the strict requirement of passing exactly through all data points. Instead, they approximate the data by minimizing residual errors, most commonly in the least-squares sense. Such approaches are generally more robust to noise and outliers, making them better suited to real-world datasets where exact measurements are rarely available (Hoffman & Frankel, 2018).

Despite the wide range of available interpolation and fitting methods, several challenges remain. Interpolation enforces exact agreement with the data points, which can lead to overfitting and oscillations, such as Runge's phenomenon. Fitting methods, by minimizing residuals, allow for smoothing but require careful selection of the model and regularization. Extending these approaches to two-dimensional surface reconstruction with sparse or irregularly spaced points is often difficult. Moreover, many classical methods struggle to systematically incorporate both equality and inequality constraints and generally lack a direct physical interpretation.

The motivation behind this study arises from the problem of reconstructing the bedrock topography of a region from sparse measurement data, such as wells or exposed bedrock outcrops, which has been the focus of subsequent studies (Kitterød, 2017; Kitterød & Leblois, 2019, 2021). To gain intuition, we first consider the one-dimensional analogue: reconstructing a smooth curve from discrete points. To this end, we employ the biharmonic equation from elasticity theory, which penalizes excessive bending and produces globally smooth solutions suitable for both one- and two-dimensional reconstructions (Szilard, 2004). Conceptually, the biharmonic equation models the deflection of a thin elastic plate or beam, and by applying appropriate constraints, it is possible to deform and generate a surface or curve that honors the given data.

In this paper, we propose a discrete biharmonic formulation for curve reconstruction, framed as a constrained quadratic optimization problem. This method naturally incorporates both equality and inequality constraints, handles irregularly spaced data, and provides a physically interpretable principle of smoothness. Moreover, it establishes a framework for surface reconstruction in higher dimensions.

The structure of this paper is as follows. Section 2 introduces the proposed curve reconstruction model. In Section 3, we detail the discretization method employed. Section 4 then presents the constrained quadratic programming approach used to solve the resulting discrete system. A discussion of performance evaluation metrics is provided in Section 5. Finally, the numerical results, discussion, and conclusion are presented in Sections 6, 7, and 8, respectively.

2 Mathematical Modeling

In this section, we explain how a smooth curve is generated from a given set of data points on the $xy-$plane. For this purpose,

let $0 \leq x_1, x_2, \ldots, x_n \leq L$ be locations of data points on the x axis and let $y_1, y_2, \ldots, y_n$ represent the corresponding measurements(exact values or bounds) along the y-axis. Our main goal is to construct a globally C^1 smooth curve that honours the given data while satisfying the specified equality and inequality constraints at each point. For this end we consider the biharmonic equation problem on $\Omega = [0, L]$:

$$u^{(4)}(x) = q(x), \text{in } \Omega, \tag{1a}$$

with Dirichlet boundary conditions

$$u(0) = y_0, \qquad u(L) = y_L, \tag{1b}$$
$$u'(0) = \alpha, \qquad u'(L) = \beta. \tag{1c}$$

In the context of beam theory, the variable u denotes the transverse deflection, while q represents the applied lateral load. The conditions given in (1b, 1c) correspond to Dirichlet boundary conditions for (1a) and physically model a beam that is clamped at both ends. Let $\partial\Omega = \partial\Omega_D$ denote the boundary of the region Ω which in this case is $\{0, L\}$.

In particular if $x_0 = 0$ and $x_n = L$, then $y_0 = y_1$ and $y_L = y_n$. Given the Sobolev space

$$\mathcal{H}^2(\Omega) = \left\{u \in L^2(\Omega) \;\middle|\; D^\alpha u \in L^2(\Omega),\ \forall |\alpha| \leq 2\right\}$$

and the subspace

$$\mathcal{H}^2_D = \{v \in \mathcal{H}^2(\Omega) : v|_{\partial\Omega_D} = v'|_{\partial\Omega_D} = 0\},$$

the variational form of (1) is:

Find $u \in \mathcal{H}^2(\Omega)$ satisfying the boundary conditions (1b), (1c) and

$$\int_\Omega u''v''dx = \int_\Omega qvdx, \quad \forall v \in \mathcal{H}^2_D. \tag{2}$$

In addition, at the given data points a set of constraints must be satisfied:

$$u(x_i) = y_i, \quad \text{for } i \in \mathcal{E}, \tag{3}$$
$$u(x_i) \leq y_i, \quad \text{for } i \in \mathcal{I}, \tag{4}$$

where $\mathcal{E}$ is the indices of the data points where the measured values are exact, and $\mathcal{I}$ the set of indices corresponding to data points where the measurements define inequality conditions. These sets are disjoint ($\mathcal{E} \cap \mathcal{I} = \phi$), allowing the reconstruction to satisfy equality conditions at $\mathcal{E}$ and inequality bounds at $\mathcal{I}$.

The idea in this curve reconstruction approach is based on the use of the discrete form of (2, 3, 4) to mimic a deflected beam satisfying the given boundary conditions and constraints provided in the data.

The weak form (2) can be written in the abstract form as: Find $u \in \mathcal{H}^2(\Omega)$ satisfying the boundary conditions (1b) such that,

$$a(u, v) = l(v), \quad \forall v \in \mathcal{H}^2_D.$$

Here $a(u, v) = \int_\Omega u''v''dx$ and $l(v) = \int_\Omega qvdx$ represent the bilinear and linear forms respectively. This weak form is equivalent to the energy minimization problem where the solution u minimizes the functional:

$$J(v) = \frac{1}{2}a(v, v) - l(v).$$

In the sense of beam theory, the quantities $\frac{1}{2}a(u, u) = \frac{1}{2}\int_\Omega (u'')^2dx$ and $l(u) = \int_\Omega q(x)u(x)dx$ represent the strain (elastic) energy and potential energy (work done by applied forces), respectively (Gavin, 2014; Szilard, 2004). The former represents the energy stored in the beam as a result of bending, quantifies the internal resistance of the material to deformation, which increases with the curvature of the beam. Since $q(x)$ is a distributed load and $u(x)$ is the deflection at the point x, the product $q(x)u(x)$ gives the infinitesimal work done by the applied force. The total energy of the system is then expressed as:

$$\Pi[u] = \frac{1}{2}\int_\Omega (u'')^2dx - \int_\Omega q(x)u(x)dx. \tag{5}$$

3 Discretization

The discrete form of (2, 3, 4) can be obtained by using the Finite Element Method (FEM) (Larson & Bengzon, 2013; Quarteroni, 2009) taking a finite dimensional function space:

$$\mathcal{V}_h = \text{Span}\{\phi_0, \phi_1, \ldots, \phi_{n_{\text{dof}}-1}\} \subset \mathcal{H}^2(\Omega),$$

where ϕ_i are suitably chosen basis (shape) functions, and n_{dof} denotes the total number of degrees of freedom (DOF). The associated subspace that satisfies the homogeneous Dirichlet boundary conditions is defined as :

$$\mathcal{V}^h_D = \{\phi \in \mathcal{V}_h : \phi = \phi' = 0, \quad \text{on } \partial\Omega\}.$$

To define the basis functions, the physical domain $\Omega = [0, L]$ is partitioned into N finite elements (subintervals) as:

$$0 = \xi_0 < \xi_1 < \xi_2 < \ldots < \xi_N = L,$$

where $h_i = x_{i+1} - x_i$ denotes the length of the ith element (for a uniform mesh, $h_i = h$). This process converts the continuous domain into a computational mesh consisting of nodes $\{x_i\}_{i=0}^N$ and elements $[x_i, x_{i+1}]$.

Within each element, local basis (shape) functions are defined, and the global basis functions $\{\phi_i(x)\}_{i=0}^{n_{\text{dof}}-1}$ are constructed by assembling the local contributions according to the mesh connectivity. These basis functions provide the finite-dimensional approximation space $\mathcal{V}_h \subset \mathcal{H}^2(\Omega)$ used for the discrete formulation.

Within this finite dimensional space, the unknown displacement $u(x)$ is approximated as a linear combination of these basis functions, as:

$$u_h(x) := \sum_{i=0}^{n_{\text{dof}}-1} c_i \phi_i(x),$$

where the coefficients c_i's are the unknown degrees of freedom(DOF) of the system.

But, for the finite element space $\mathcal{V}_h$ to be a valid subspace of $\mathcal{H}^2(\Omega)$, the minimum requirement on its basis function is C^1 continuity. This ensures, the functions as well as their weak first and second derivatives be square integrable across elements boundary, hence belong to $\mathcal{H}^2$.

To determine these basis functions in a reference element, completeness and compatibility requirements (Ottosen & Petersson, 1991) indicate that the element level deflection u^e must be expressed as:

$$u^e(x) = \alpha_0 + \alpha_1 x + \alpha_2 x^2 + \alpha_3 x^3, \quad x \in [\xi_i, \xi_{i+1}].$$

Taking the displacement and slope DOF at the ends $u^e(0) = u_i, (u^e)'(0) = \theta_i, u^e(h) = u_{i+1}, (u^e)'(h) = \theta_{i+1}$, we can show that

$$u^e(x) = \mathbf{N}^e(x)\mathbf{d}^e,$$

where

- $\mathbf{d}^e = [u_i, \theta_i, u_{i+1}, \theta_{i+1}]^T$ is the vector of nodal DOFs (displacements u and slope θ),
- $\mathbf{N}^e(x) = [\phi_1^e(x), \phi_2^e(x), \phi_3^e(x), \phi_4^e(x)]$ is the row vector of shape functions.

Moreover the element basis functions are given in closed form as:

$$\phi_1^e(x) = 1 - 3\frac{x^2}{h^2} + 2\frac{x^3}{h^3}, \qquad \phi_3^e(x) = \frac{x^2}{h^2}\left(3 - 2\frac{x}{h}\right),$$
$$\phi_2^e(x) = x\left(1 - 2\frac{x}{h} + \frac{x^2}{h^2}\right), \quad \phi_4^e(x) = \frac{x^2}{h}\left(\frac{x}{h} - 1\right).$$

Two basis function at each grid node of the mesh are generated one for the displacement and one for the slope. The global basis functions are then defined using two adjacent element basis functions and zero in all other elements. In Fig. 1 the domain $[0, L]$ is discretized into five subintervals and a total of twelve global basis functions are defined: four $(\phi_0, \phi_1, \phi_{10}, \phi_{11})$ correspond to boundary basis functions, while for the internal nodes, ϕ_i with even i represent displacement DOFs and the remaining functions correspond to slope DOFs at each node.

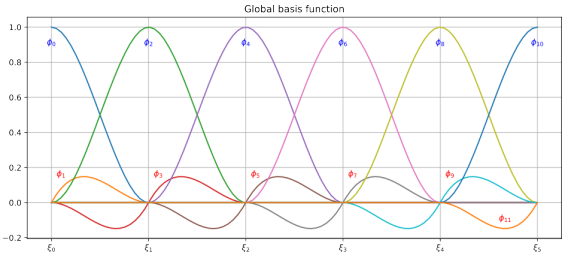

Figure 1: Graphical illustration of the global basis functions. The domain is subdivided into five elements with six nodes.

In this way, we construct the nodal displacement basis functions ϕ_{2i} and the nodal derivative basis functions ϕ_{2i+1} for $i = 0, \ldots, N$, giving a total of $2(N+1)$ degrees of freedom. These functions satisfy the interpolation conditions:

$$\phi_{2i}(\xi_j) = \delta_{ij}, \quad \phi'_{2i}(\xi_j) = 0, \quad \phi_{2i+1}(\xi_j) = 0, \quad \phi'_{2i+1}(\xi_j) = \delta_{ij}, \quad \forall i, j,$$

with $\delta_{i,j}$ representing the Kronecker delta function of two integres i, j defined as:

$$\delta_{ij} = \begin{cases} 1 & (i = j) \\ 0 & (i \neq j) \end{cases}.$$

Replacing u with u_h and v by an arbitrary function $\phi_j \in \mathcal{V}_D^h$ we arrived at the discretized formulation as:

$$\sum_{i=0}^{n_{\text{dof}}-1} c_i \int_\Omega \phi_i'' \phi_j'' dx = \int_\Omega q\phi_j dx, \quad j \in \mathcal{J}, \tag{6}$$

such that:

$$\sum_{i=0}^{n_{\text{dof}}-1} c_i \phi_i(x_k) = y_k, \quad \text{for } k \in \mathcal{E}, \tag{7}$$
$$\sum_{i=0}^{n_{\text{dof}}-1} c_i \phi_i(x_k) \leq y_k, \quad \text{for } k \in \mathcal{I}, \tag{8}$$

where $\mathcal{J}$ represent the set of indexes of basis functions $\phi_j \in \mathcal{V}_D^h$.

This can be written in matrix form as:

$$A\mathbf{x} = \mathbf{b}, \tag{9a}$$
$$C\mathbf{x} = \mathbf{d}, \tag{9b}$$
$$E\mathbf{x} \leq \mathbf{e}, \tag{9c}$$

with $\mathbf{x}$ is the vector of degrees of freedom of u_h. Here, the matrix A represents the corresponding stiffness matrix, which is symmetric and positive definite; $\mathbf{b}$ is the load vector. The constraint matrices C (equality) and E (inequality) consist of basis function values at the respective data locations. Since the basis functions possess local support and all data points are distinct, both C and E are guaranteed to have full row rank. As the boundary is of Dirichlet type the DOF $c_0, c_1, c_{n_{\text{dof}}-2}$ and $c_{n_{\text{dof}}-1}$ are specified in (9).

In some practical applications, the values or derivatives at the boundaries may be unspecified. If the boundary derivative values $u'(0)$ and $u'(L)$ are unknown, the corresponding degrees of freedom in the approximate solution u_h are c_1 and $c_{n_{\text{dof}}-1}$. These can then be treated as unknowns and estimated by solving the discrete system (9). Similarly, if the derivatives are known

but the boundary displacements $u(0)$ and $u(L)$ are unknown, the corresponding degrees of freedom c_0 and $c_{n_{\text{dof}}-2}$ can be estimated from the same system.

4 Constrained Quadratic Programming Approach

From the discretization of the continuous form, we arrive at a system of equations and inequalities (9). In general, this system is overdetermined and may also include inequality constraints. From the outset, our goal has been to construct a globally smooth (C^1) curve based on the concept of bending beams. By the nature of beam deflection, it is evident that at equilibrium a beam bends to minimize its total energy (5), comprising both internal and external contributions. In the discrete formulation, these are represented by $\frac{1}{2}\mathbf{x}^T A\mathbf{x}$ (internal energy) and $-\mathbf{x}^T\mathbf{b}$ (external energy), with the total energy given by:

$$J(\mathbf{x}) = \frac{1}{2}\mathbf{x}^T A\mathbf{x} - \mathbf{x}^T\mathbf{b}.$$

Consequently, we choose to solve the system using a constrained quadratic programming (QP) formulation:

$$\begin{aligned} \min_{\mathbf{x}} \quad & \frac{1}{2}\mathbf{x}^T A\mathbf{x} - \mathbf{b}^T\mathbf{x}, && \text{(10a)} \\ \text{subject to} \quad & C\mathbf{x} = \mathbf{d}, && \text{(10b)} \\ & E\mathbf{x} \leq \mathbf{e}. && \text{(10c)} \end{aligned}$$

This structure makes the problem a natural candidate for quadratic programming as the objective is quadratic (bending energy), ensuring smoothness,the equality constraints guarantee interpolation and exact boundary enforcement and the inequality constraints provide flexibility to incorporate additional physical or geometric requirements. Practically the quadratic programming problem is solved in Python using the cvxpy package with the OSQP solver, an operator splitting method designed for convex quadratic programs with linear equality and inequality constraints.

In particular, when $\mathcal{I} = \{\}$, i.e., with no inequality constraint, the problem (10) reduced to interpolation and has the lagrangian

$$\mathcal{L}(\mathbf{x}, \lambda) = \frac{1}{2}\mathbf{x}^T A\mathbf{x} - \mathbf{b}^T\mathbf{x} + \lambda^T(C\mathbf{x} - \mathbf{d}).$$

Using the first-order optimality condition on $\mathcal{L}$, i.e., $\frac{\partial \mathcal{L}}{\partial \mathbf{x}} = \frac{\partial \mathcal{L}}{\partial \lambda} = 0$, we have the normal equation, i.e. the Karush–Kuhn–Tucker (KKT) system, for quadratic programming problem:

$$\underbrace{\begin{bmatrix} A & C^T \\ C & 0 \end{bmatrix}}_{\mathbf{M}} \begin{bmatrix} \mathbf{x} \\ \boldsymbol{\lambda} \end{bmatrix} = \underbrace{\begin{bmatrix} \mathbf{b} \\ \mathbf{d} \end{bmatrix}}_{\mathbf{rhs}}. \qquad (11)$$

Existence of reconstructed curve:

Since the stiffness matrix A is symmetric positive definite, the objective function is strictly convex. The equality constraint matrix $C \in \mathbb{R}^{|\mathcal{E}| \times n_{\text{dof}}}$, from the local support nature of the basis functions and distinct data point locations, has full row rank. This implies that the linear map $C : \mathbb{R}^{n_{\text{dof}}} \to \mathbb{R}^{|\mathcal{E}|}$ is surjective. Consequently, for any prescribed right-hand side $\mathbf{d} \in \mathbb{R}^{|\mathcal{E}|}$, the constraint $C\mathbf{x} = \mathbf{d}$ defines a nonempty affine subspace, i.e., a feasible region.

Minimizing a strictly convex function over a nonempty affine set guarantees the existence and uniqueness of the minimizer $[\mathbf{x}, \boldsymbol{\lambda}]^T$. Equivalently, the associated KKT matrix (11) is nonsingular. Because the reconstructed curve u_h is obtained from $\mathbf{x}$ through a linear combination of the basis functions, the resulting curve is unique within the chosen approximation space. This establishes the well-posedness of the reconstruction step.

Dynamic Adaptation of the Method:

The method is able to update the solution incrementally when new data points are added. For example, if a single data point is added, this corresponds to a constraint of the form $C_{\text{new}}\mathbf{x} = \mathbf{d}_{\text{new}}$, resulting in the KKT system

$$\underbrace{\begin{bmatrix} A & C^T & C_{\text{new}}^T \\ C & 0 & 0 \\ C_{\text{new}} & 0 & 0 \end{bmatrix}}_{\mathbf{M}_{\text{new}}} \begin{bmatrix} \mathbf{x} \\ \boldsymbol{\lambda} \\ \boldsymbol{\lambda}_{\text{new}} \end{bmatrix} = \underbrace{\begin{bmatrix} \mathbf{b} \\ \mathbf{d} \\ \mathbf{d}_{\text{new}} \end{bmatrix}}_{\mathbf{rhs}_{\text{new}}}. \qquad (12)$$

The structure of $\mathbf{M}_{\text{new}}$ indicates that the system does not need to be rebuilt from scratch when a new data point is added. Instead, we append C_{new} to the original matrix $\mathbf{M}$ and $\mathbf{d}_{\text{new}}$ to the right-hand side vector. This makes the method dynamically updatable and significantly reduces computational cost.

Since the problem has a unique solution, it can be formally obtained as $\mathbf{M}_{\text{new}}^{-1}\mathbf{rhs}_{\text{new}}$. However, the computation of $\mathbf{M}_{\text{new}}^{-1}$ can be efficiently performed using the block matrix inverse formula:

$$\begin{aligned} \mathbf{M}_{\text{new}}^{-1} &= \begin{pmatrix} \mathbf{M} & B^T \\ B & 0 \end{pmatrix}^{-1}, \quad B = \begin{pmatrix} C_{\text{new}} & 0 \end{pmatrix}, \\ &= \begin{pmatrix} \mathbf{M}^{-1} - \mathbf{M}^{-1}B^T S^{-1} B\mathbf{M}^{-1} & \mathbf{M}^{-1}B^T S^{-1} \\ S^{-1}B\mathbf{M}^{-1} & -S^{-1} \end{pmatrix}, \\ S &= B\mathbf{M}^{-1}B^T. \end{aligned}$$

This expression is entirely in terms of the original inverse $\mathbf{M}^{-1}$ and the new constraint C_{new}. The Schur complement $S = B\mathbf{M}^{-1}B^T = C_{\text{new}}XC_{\text{new}}^T$, where X is the top-left block of $\mathbf{M}^{-1}$. The invertibility of S is guaranteed as long as the rows of C_{new} are linearly independent of the rows of C.

Let

$$\mathbf{V}_{\text{old}} = \begin{pmatrix} \mathbf{x}_{\text{old}} \\ \boldsymbol{\lambda}_{\text{old}} \end{pmatrix} = \mathbf{M}^{-1}\mathbf{rhs} = \begin{pmatrix} X & Y \\ Z & W \end{pmatrix} \mathbf{rhs},$$

be the solution of the original system (11). Then the solution of the updated system (12) can be expressed as

$$\boldsymbol{\lambda}_{\text{new}} = S^{-1}(C_{\text{new}}\mathbf{x}_{\text{old}} - \mathbf{d}_{\text{new}}), \tag{13a}$$

$$\mathbf{x} = \mathbf{x}_{\text{old}} - XC_{\text{new}}^{T}\boldsymbol{\lambda}_{\text{new}}, \tag{13b}$$

$$\boldsymbol{\lambda} = \boldsymbol{\lambda}_{\text{old}} - ZC_{\text{new}}^{T}\boldsymbol{\lambda}_{\text{new}}. \tag{13c}$$

The solution formula (13) has a recurrence-like structure: each time a new constraint is added, the updated solution is obtained from the previous solution plus a correction depending only on the new constraint. This allows the solution to be incrementally updated without re-solving the entire system, and sequential additions produce a chain of solutions that grow with the number of constraints.

5 Model Evaluation

The performance of the proposed method is evaluated using approaches, combining quantitative error metrics with qualitative assessment. To establish accuracy, we first validate the method against a known analytical function. This provides a benchmark for quantifying error through several metrics, including the L^2 norm for overall fit, the L^∞ norm for the maximum pointwise deviation, and the L^2 norm of the derivative error to assess smoothness and physical plausibility of the reconstructed curve. In addition, the normalized root mean square error (NRMSE) is employed for scale independent comparison.

In addition to these quantitative metrics, qualitative assessment is conducted by visually inspecting the reconstructed curves. This includes examining the ability of the method to accurately interpolate equality constraints, respect inequality bounds, maintain smoothness across the domain, and avoid spurious oscillations. Visual comparisons are also made between the reconstructed curves and classical interpolators, such as cubic splines, under both uniform and irregular sampling, as well as in the presence of small perturbations in the input data.

Formally, let f denote the exact function and g the reconstructed curve obtained using the proposed approach. The error function is defined as $e(x) = f(x) - g(x)$. The following metrics are considered to capture different aspects of the error, including function values, derivatives, and integral properties:

- **Normalized Root Mean Square Error (NRMSE):**

$$\text{NRMSE} = \frac{1}{f_{max} - f_{min}}\sqrt{\sum_{i=1}^{N}\frac{(f(\xi_i) - g(\xi_i))^2}{N}}.$$

- L^∞ **Norm of the Error (L^∞- Error):** Also known as the maximum error, it measures the largest pointwise deviation.

$$||e||_\infty = ||f - g||_\infty = \sup_{x\in[0,L]} |f(x) - g(x)|.$$

- L^2 **Norm of the Error (L^2-Error):** Measures the mean-squared difference between the two curves. Smaller values indicate a better overall fit.

$$||e||_2 = ||f - g||_2 = \sqrt{\int_0^L (f(x) - g(x))^2\, dx}.$$

- L^2 **Norm of the First Derivative Error:** Evaluates how well the slope of the reconstructed curve matches the slope of the exact curve.

$$||e'||_2 = ||f' - g'||_2 = \sqrt{\int_0^L (f'(x) - g'(x))^2\, dx}.$$

Beyond numerical accuracy, the robustness of the method is also examined. In cases where the exact function is unknown, stability is assessed by introducing small random perturbations to the input data and verifying that the reconstruction remains consistent. Furthermore, the method's performance can be systematically evaluated under different point distributions, including uniformly spaced, irregularly spaced, and clustered points. Finally, all reconstructions are subject to visual inspection to ensure physical plausibility and to confirm the absence of spurious oscillations.

Sensitivity analysis can also be performed for the problem (10) to examine how small perturbations in the measurement data $\mathbf{d}$ affect the solution $\mathbf{x}$. Let $\mathbf{x}^*$ be the optimal primal solution of the unperturbed problem, and let $\boldsymbol{\lambda}^*$ and $\boldsymbol{\mu}^*$ be the optimal dual multipliers for the equality and inequality constraints, respectively. Define the active set

$$\mathcal{A} = \{\, i : E_i\mathbf{x}^* = \mathbf{e}_i \,\},$$

where E_i and $\mathbf{e}_i$ denote the i^{th} row of the matrix E and the i^{th} entry of the vector $\mathbf{e}$, respectively.

Suppose a small perturbation $\Delta\mathbf{d}$ is applied to $\mathbf{d}$, and assume that the active set $\mathcal{A}$ remains unchanged. The corresponding perturbed solution becomes $\mathbf{x}^* + \Delta\mathbf{x}$, with dual multipliers $\boldsymbol{\lambda}^* + \Delta\boldsymbol{\lambda}$ and $\boldsymbol{\mu}^*_{\mathcal{A}} + \Delta\boldsymbol{\mu}_{\mathcal{A}}$. Subtracting the KKT systems of the perturbed and unperturbed problems yields the linearized system

$$\underbrace{\begin{pmatrix} A & C^T & E_{\mathcal{A}}^T \\ C & 0 & 0 \\ E_{\mathcal{A}} & 0 & 0 \end{pmatrix}}_{\mathbf{K}} \begin{pmatrix} \Delta\mathbf{x} \\ \Delta\boldsymbol{\lambda} \\ \Delta\boldsymbol{\mu}_{\mathcal{A}} \end{pmatrix} = \begin{pmatrix} \mathbf{0} \\ \Delta\mathbf{d} \\ \mathbf{0} \end{pmatrix}.$$

Thus,

$$\begin{pmatrix} \Delta\mathbf{x} \\ \Delta\boldsymbol{\lambda} \\ \Delta\boldsymbol{\mu}_{\mathcal{A}} \end{pmatrix} = \mathbf{K}^{-1}\begin{pmatrix} \mathbf{0} \\ \Delta\mathbf{d} \\ \mathbf{0} \end{pmatrix} = \begin{pmatrix} \mathbf{K}_{11} & \mathbf{K}_{12} & \mathbf{K}_{13} \\ \mathbf{K}_{21} & \mathbf{K}_{22} & \mathbf{K}_{23} \\ \mathbf{K}_{31} & \mathbf{K}_{32} & \mathbf{K}_{33} \end{pmatrix}\begin{pmatrix} \mathbf{0} \\ \Delta\mathbf{d} \\ \mathbf{0} \end{pmatrix},$$

and we obtain

$$\Delta \mathbf{x} = \mathbf{K}_{12}\, \Delta \mathbf{d} = J\, \Delta \mathbf{d}, \tag{14}$$

where $J = \frac{\partial \mathbf{x}^*}{\partial \mathbf{d}}$ is the Jacobian of the optimal solution with respect to the data $\mathbf{d}$.

From (14), we see that the perturbation in the solution is linearly related to the perturbation in the input data.

Let

$$G = \begin{pmatrix} C \\ E_{\mathcal{A}} \end{pmatrix}, \qquad S = -GA^{-1}G^T, \qquad S^{-1} = \begin{pmatrix} S_{11}^{-1} & S_{12}^{-1} \\ S_{21}^{-1} & S_{22}^{-1} \end{pmatrix}.$$

Then the sensitivity matrix J admits the explicit form

$$J = \begin{cases} A^{-1}C^T(CA^{-1}C^T)^{-1}, & \text{if } \mathcal{A} = \varnothing, \\ -A^{-1}\big(C^T S_{11}^{-1} + E_{\mathcal{A}}^T S_{21}^{-1}\big), & \text{otherwise.} \end{cases}$$

Using the linear relation (14), for a set of perturbations $\{\Delta \mathbf{d}^{(k)}\}_{k=1}^{K}$ and the resulting perturbations in the solution $\{\Delta \mathbf{x}^{(k)}\}_{k=1}^{K}$, we may compute the maximum deviation at each grid point, $\max_k |\Delta \mathbf{x}_i^{(k)}|$, the standard deviation $\sigma_x = \text{std}\{\Delta \mathbf{x}^{(k)}\}$, and visualize the corresponding 95% confidence interval about the optimal solution $\mathbf{x}^*$.

6 Results

In this section, we use the discrete biharmonic curve reconstruction method under a variety of scenarios. The results are organized to show the method's flexibility in handling different types of constraints and boundary conditions, as well as its accuracy compared to classical interpolation technique. For each of this result the lateral load q is chosen to be zero. We consider the following cases:

- Reconstruction with only equality constraints at the given data points, illustrating the ability of the method to exactly interpolate the known values.
- Reconstruction with both equality and inequality constraints at selected points, demonstrating the method's capability to enforce bounds on the solution.
- Validation of the method using data sampled from known analytical functions, to quantify the accuracy and robustness of the reconstructed curves.
- Observe the stability of the resulting curve reconstruction for small perturbation in the data points.

Imposed conditions

Reconstruction of a curve using the proposed method in the presence of equality and/or inequality conditions at data points and specified boundary condition.

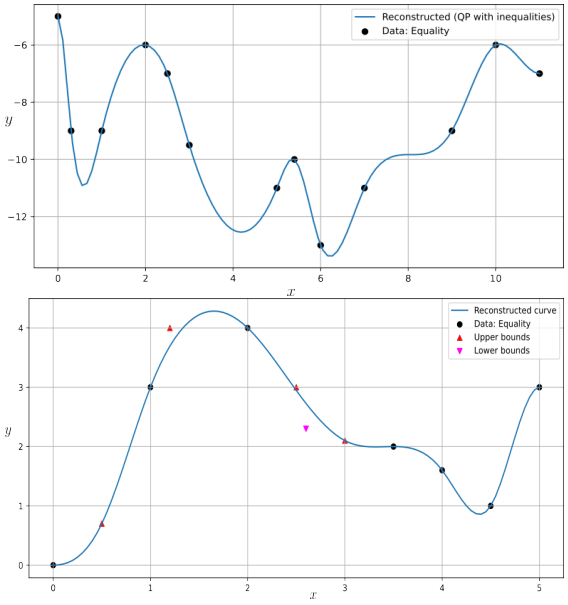

Figure 2: Plot of the curve reconstructed using the discrete biharmonic approach for the case of a randomly chosen data consisting of only equality conditions (*Left*) and for the case where data contain both equality, lower bound and upper bound at some locations (*Right*).

As shown in Fig.2, for the given set of synthetic data points and specified Dirichlet boundary conditions (DBCs), the proposed method generates a curve that passes through all interpolation points, satisfies the prescribed lower bound, upper bound constraint, and enforces known Dirichlet boundary conditions as expected. In particular, the reconstructed curve in Fig. (2, *Right*) the interpolation points are with coordinates $(x_{\text{data}}, y_{\text{data}}) = ([0,\ 1,\ 2,\ 3.5,\ 4,\ 4.5,\ 5],\ [0,\ 3,\ 4,\ 2,\ 1.6,\ 1,\ 3])$, the location of the upper bounds are at $x_{up} = [0.5, 1.2, 2.5, 3]$ with values $y_{up} = [0.7, 4, 3, 2.1]$, location and values for the lower bound is $x_{lb} = [2.6], y_{lb} = [2.3]$ and the derivates at the ends are zero.

For this data, the resulting curve has values $[0, 3, 4, 2, 1.6, 1, 3]$ at the interpolation, $[0.7, 3.63, 2.63, 1.65]$ at the upper bound locations and $[2.34]$ at lower bound. The results indicate the interpolation constraints are satisfied exactly. The reconstructed value at the lower bound location exceeds the required minimum of 2.3, and the values at the upper bound locations remain below or equal to the specified limits. This demonstrates that the method can simultaneously interpolate given data and honor inequality constraints, producing a curve that is both accurate and physically consistent.

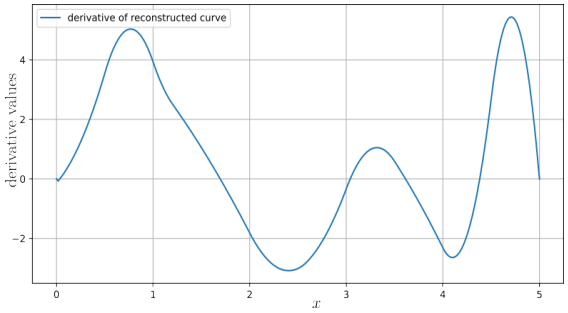

Figure 3: Plot of the derivative of the reconstructed curve(Fig: 2; *Right*)

In addition, the smoothness requirement is confirmed by examining the derivative of the reconstructed curve. As shown in Fig. 3, the derivative is continuous, indicating that the reconstructed curve possesses a continuous first derivative and therefore belongs to the class C^1. Moreover, the boundary derivative conditions, which are zero at both ends in this case, are also satisfied exactly, as evident from the figure.

In some practical applications, the endpoint derivatives are typically unknown leading to presence of unspecified Dirichlet boundary conditions. An estimate of these can be obtained from the solution of the discrete system.

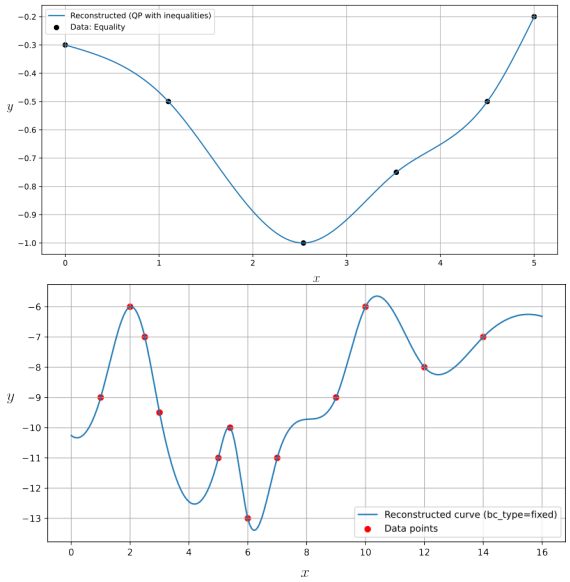

Figure 4: Reconstructed curve from a given set of data points where the endpoint derivatives(*Left*) and values(*Right*) are not prescribed and are instead estimated.

Performance of the proposed method

To assess the performance of the proposed method, data points are taken from known representative functions. For each case, visual comparison of the exact curve, the reconstruction produced by our method, and a standard *cubic spline* interpolator, are shown in Fig. 5. Data points are taken from a known function: $f(x) = \sin(x)$ with irregularly spaced points *Left* and Bessel function of the first kind of order zero $J_0(\sqrt{x})$ with regularly spaced points *Right*.

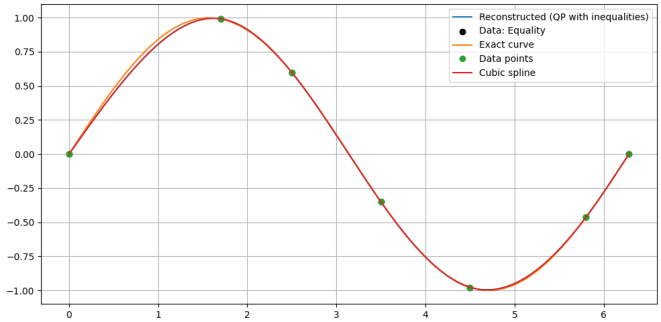

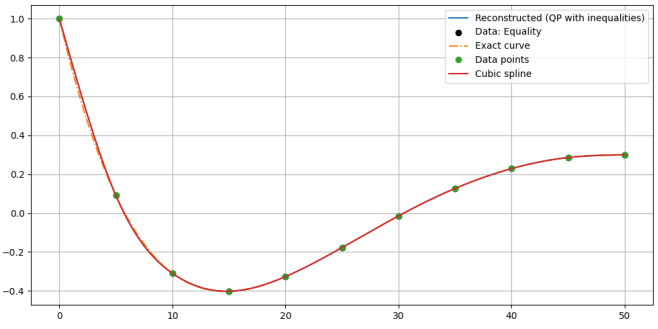

Figure 5: Visual comparison of the proposed method with the cubic spline.

Additional functions from different classes are selected to further evaluate the method, each representing a distinct curve behavior. For each function, performance metrics are computed using uniformly spaced data points, and the results are reported in Table 1. The trapezoidal rule was employed to approximate the integrals appearing in the matrices. The reported error norm values(maximum norm, L^2 norm of the error) can be normalized and interpreted as percentages relative to the range.

Stability

The influence of small perturbations in the input data on the reconstructed curve gives important indication of the stability of the proposed method. To examine this, we introduce random noise of small magnitude to the y-values of the sampled points and analyze the corresponding changes in the reconstructed curve. Both uniformly spaced and non uniformly spaced data points are considered to assess the method's resilience under different sampling patterns. In Fig. 6 and 7 data points are taken from the function $f(x) = \frac{1}{1+25x^2}$ and small perturbations are applied to the corresponding y_i's.

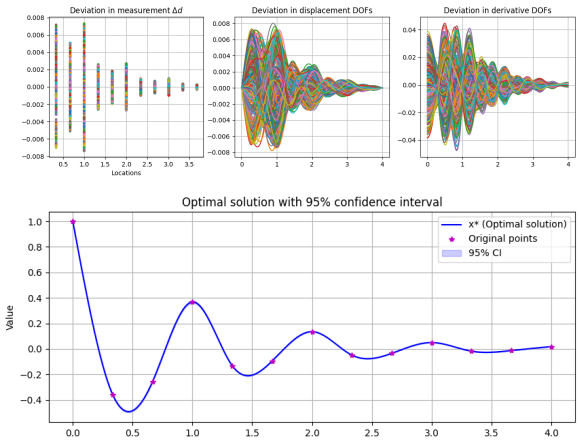

Figure 6: Effect of small perturbations Δd's on the reconstructed curve with 95% confidence interval: equally spaced points.

Table 1: Performance of the proposed approach for data points sampled uniformly from known analytic functions. Here, n denotes the number of data points.

f	L	n	Range(f)	NRMSE	$\|\|e\|\|_\infty$	$\|\|e\|\|_{L^2}$	$\|\|e'\|\|_{L^2}$
$J_0(\sqrt{x})$	50	11	1.403	0.006	0.038	0.060	0.10
$x^3 - 4x^2 + 3x$	3	10	2.744	0.006	0.054	0.029	0.30
$\sin(x)$	2π	7	2.000	0.007	0.010	0.036	0.07
$\frac{1}{1+25x^2}$	1	8	0.962	0.001	0.002	0.001	0.029
$e^{-x}\cos(2\pi x)$	4	13	1.614	0.011	0.060	0.036	0.35

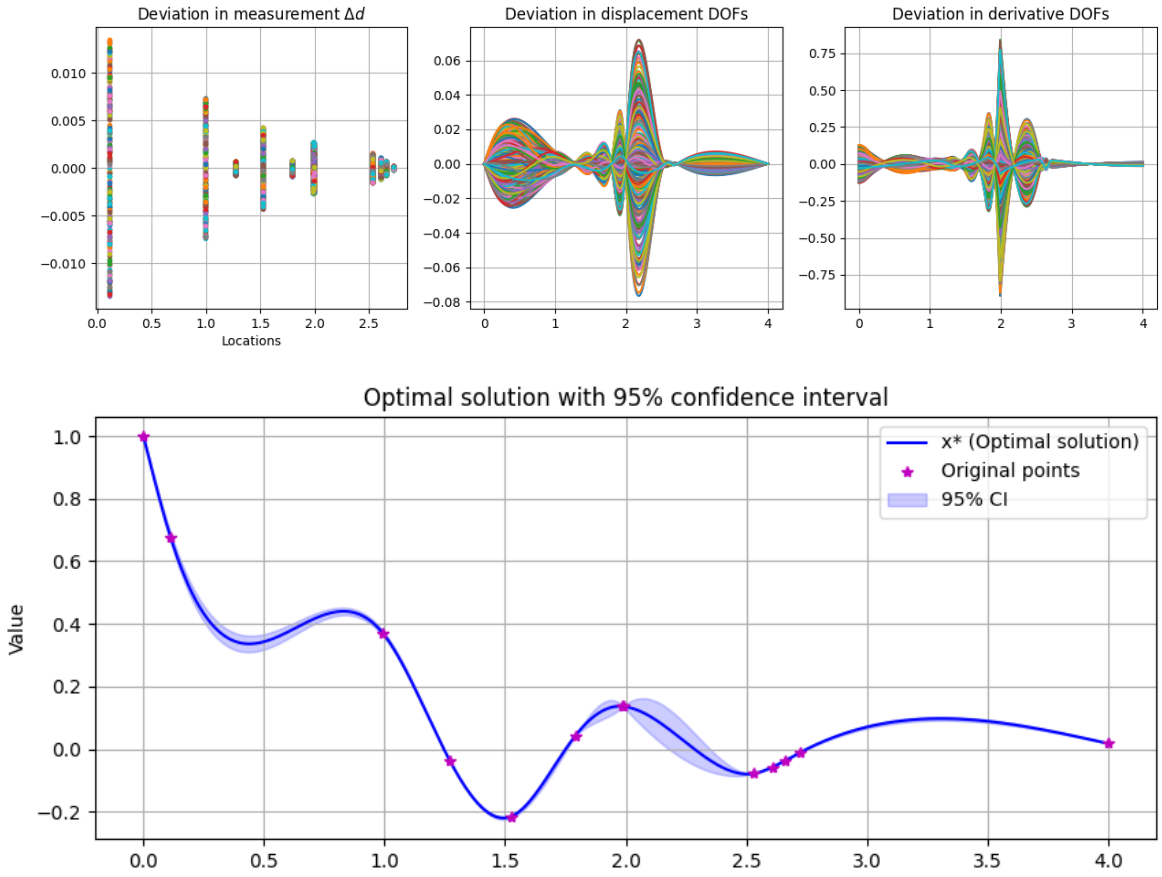

Figure 7: Effect of small perturbations in Δd's on the reconstructed curve with 95% confidence interval: unequally spaced points.

7 Discussion

An important aspect of the proposed method is its ability to flexibly accommodate different types of requirements while maintaining smoothness. *First*, it exactly interpolates through the equality data points, ensuring that the reconstructed curve honors all available information. *Second*, it is capable of satisfying inequality constraints, such as prescribed upper/lower bounds, demonstrating its ability in incorporating additional problem specific requirements. *Third*, the method consistently enforces the given boundary conditions, whether Dirichlet or Mixed, without having unnecessary oscillations near the boundaries.

Finally, by construction, the discrete biharmonic formulation produces curves that are not only honor conditions at the data points but also smooth, with continuity in the first derivative. This combination of physical interpretability, interpolation, constraint enforcement, boundary adherence and smoothness makes the approach well suited for practical applications where multiple conditions must be satisfied simultaneously.

From the NRMSE values in Table 1, we observe that the maximum deviation of the reconstructed curves from the exact functions is less than 1%. These results indicate that the proposed discrete biharmonic approach provides a robust and highly accurate method for curve reconstruction from the given data points. The consistently low NRMSE values (e.g., < 0.01) across diverse test functions demonstrate strong global fidelity, showing that the reconstructed curves are, on average, very close to the exact curves.

Furthermore, small L^∞ errors (e.g., < 0.06) provide evidence of local stability, confirming that no significant localized deviations or unwanted oscillations occur. This represents an

improvement over classical high order polynomial interpolation, which is known to suffer from instabilities such as the Runge's phenomenon.

The absolute error norms further demonstrate the accuracy of the proposed method. The L^2-errors remain small across all tested functions, with values ranging between 0.001 and 0.060, showing that the reconstructed curves are too close to the originals in terms of global shape. In contrast, the derivative errors are relatively larger (0.029–0.35). For instance, the oscillatory function $e^{-x}\cos(2\pi x)$ exhibits the highest derivative error (0.35), while smoother functions such as $\frac{1}{1+25x^2}$ yield much lower errors (0.029).

Further investigation in to the L^2 norm of the derivative of the proposed approach and the cubic interpolator over the same FEM grid shows that for the first three functions both methods have almost the same error values (L^2 norm of the value as well as derivative) where as for the last two cases the cubic spline has large error values of 2.10 and 1.135 respectively.

The robustness of the proposed method was further demonstrated through tests involving small perturbations to the input data. By adding random noise to the sampled points, we observed in Figs. 6, 7 that the largest deviation in the solution are 0.008 and 0.06 for the case of equally spaced and unequally spaced data points respectively. This shows the reconstructed curves remained very close to the one obtained from the unperturbed data.

The perturbation is introduced as follows. For each constraint d_j, the maximum error magnitude S_j is first set to 2% of its given value, that is, $S_j = 0.02\,|d_j|$. In this way, constraints with larger absolute values are allowed to have proportionally larger absolute errors.

In each trial k, the perturbation $\Delta d^{(k)}$ is generated by multiplying S elementwise by a random vector $\mathbf{r}$, where each component r_j is drawn independently from a uniform distribution over the interval $[-1, 1]$. Consequently, each entry of Δd (say Δd_j) lies within the range $[-S_j, S_j]$.

Table 2 quantifies this effect: across all considered functions, the maximum deviation (L_∞) is below 0.12, the mean absolute error (MAE) remains around 0.02–0.04, and the normalized RMSE (NRMSE) does not exceed 2.4%. This demonstrates that, rather than amplifying measurement errors, the discrete biharmonic formulation effectively smooths out minor fluctuations while preserving the global shape of the curve. Importantly, the absence of spurious oscillations in the perturbed reconstructions confirms that the method can reliably handle imperfect or noisy data, a feature that is crucial for practical applications where measurement errors are unavoidable.

Table 2: Maximum norm, MAE, and NRMSE for the deviation of the reconstructed curve from the original curve due to perturbations in the data values; uniformly spaced data points.

f	$\|\|\cdot\|\|_\infty$	MAE	NRMSE (%)
$J_0(\sqrt{x})$	0.04	0.02	1.49
$x^3 - 4x^2 + 3x$	0.12	0.04	2.03
$\sin(x)$	0.07	0.03	1.54
$\frac{1}{1+25x^2}$	0.04	0.02	2.39
$e^{-x}\cos(2\pi x)$	0.06	0.02	1.50

Comparison with some known methods:
To further validate the efficacy of the proposed biharmonic approach, we conducted a comparative analysis against well-established interpolation and regression methods, including Kriging, Radial Basis Function (RBF) interpolation, and Gaussian Process Regression (GPR).

Specifically, Kriging and GPR are rooted in stochastic processes and provide uncertainty quantification, while RBFs are deterministic kernel-based interpolators. Figure 8 illustrates the performance of these methods for data points sampled from a known analytic function, considering both uniformly and non-uniformly spaced sampling. A quantitative assessment of the performance metrics, based on the Mean Absolute Error (MAE), Root Mean Square Error (RMSE), and maximum error norms (L^∞), is provided in Table 3.

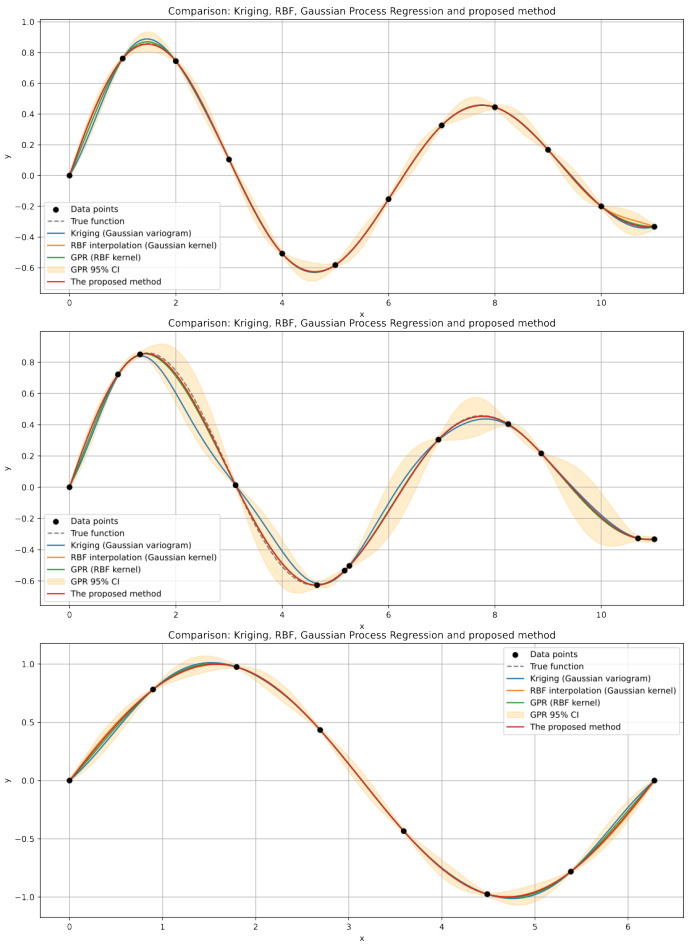

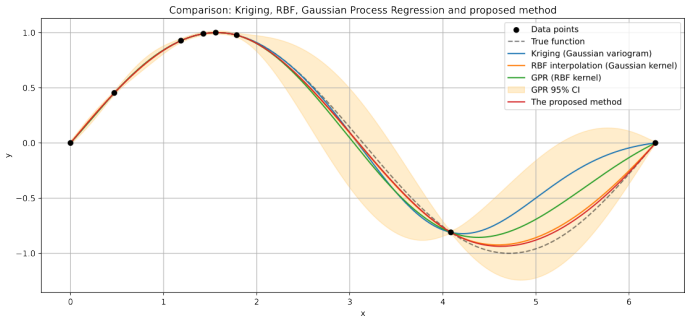

Figure 8: Comparison of the proposed approach in relation to kriging, radial basis function and gaussian process regression methods for points picked from $e^{-0.1x}\sin(x)$ (*Top*) and $\sin(x)$ (*Bottom*).

Effect of discretization size:

The effect of discretization size on the accuracy of the reconstructed curve is illustrated in Fig. 9 for the functions $e^{-0.1x}\sin(x)$ and $\sin(x)$, using uniformly spaced data points as summarized in Table 3. For both examples, the error metrics initially vary with mesh refinement but eventually reach a plateau, indicating that the solution becomes nearly independent of the discretization size. This flattening behavior demonstrates that the reconstruction method attains numerical stability beyond a certain resolution, and further mesh refinement yields negligible improvement in accuracy.

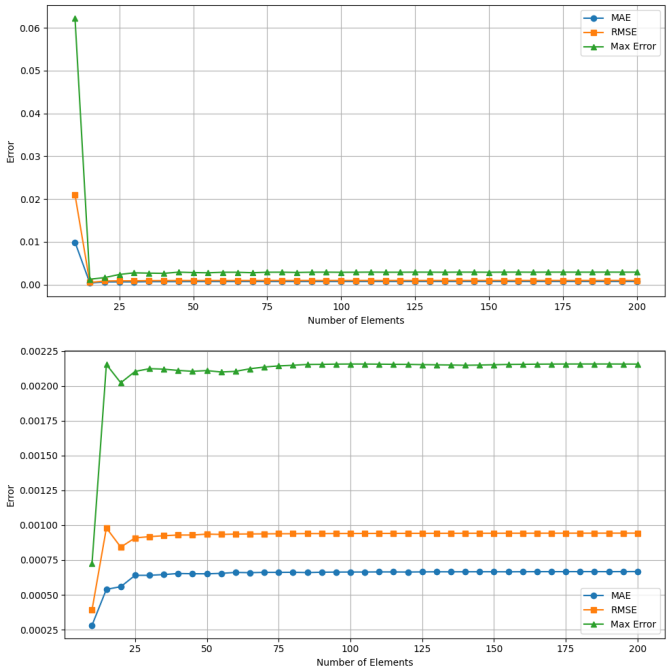

Figure 9: Effect of mesh density (step size) on the proposed curve reconstruction.

The conditioning of the discrete system was also examined for grids ranging from 10 to 200 elements. The condition number increased from approximately 10^3 on coarse meshes to around 10^7 on the finest mesh. This behavior is consistent with the theoretical properties differential operators, whose discretizations naturally become more ill-conditioned as the mesh is refined.

Despite these strengths, the accuracy of the proposed method depends strongly on the distribution and density of input data points. In sparsely sampled regions, the reconstructed curve may fail to capture local variations, while closely spaced points can induce localized oscillations due to strict enforcement of pointwise constraints. Being deterministic, the method does not account for data uncertainty or spatial correlations, which are often important in spatial interpolation to leverage information from neighboring observations.

Surface reconstruction case:

The scalability of the proposed approach to surface reconstruction is illustrated in Fig. 10 with homogeneous Dirichlet boundary condition and interior data point location [(0.3, 0.2), (0.2, 0.7), (0.7, 0.2), (0.8, 0.63), (0.5, 0.7), (0.45, 0.45), (0.52, 0.61)] and the corresponding z values [0.2, 0.1,-0.23, 0.32, -0.2, -0.15, 0.12]. The computational domain is discretized using the DUNE (Bastian et al., 2021) software, whereas the weak form of the governing equations is approximated using the Virtual Element Method (VEM) (Beirão da Veiga et al., 2013; Brezzi & Marini, 2013). The Figure shows both the projection of the reconstructed surface onto the xy-plane (left) and its three-dimensional representation (right). Moreover, this surface reconstruction approach has been applied to the estimation of bedrock topography, as presented in (Bekele et al., 2025), with additional results forthcoming.

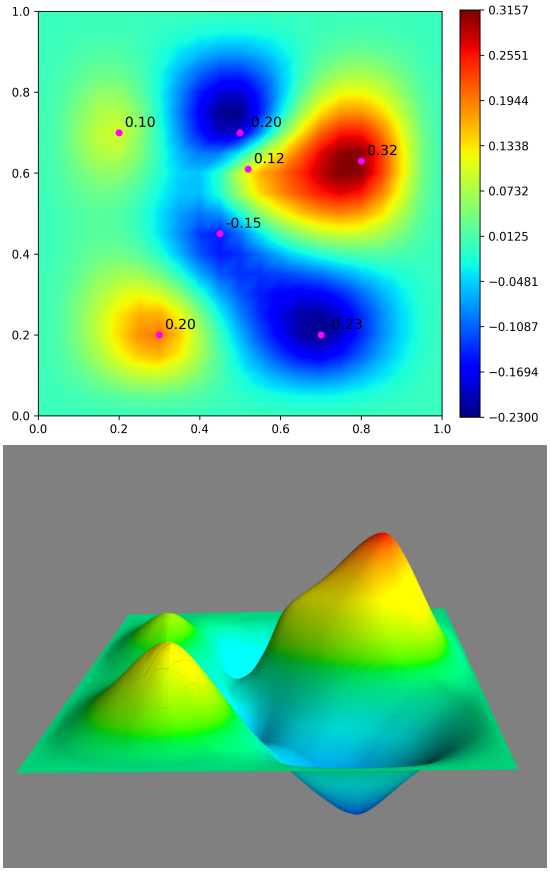

Figure 10: Surface reconstruction from a given set of data points using the extension of the proposed approach.

Table 3: Error comparison for the two functions under uniform and non-uniform sampling illustrated in Fig. 8.

Example	Data Type	Method	MAE	RMSE	Max Norm
Ex1: $\sin(x)e^{-0.1x}$ $x \in [0, 11]$	Uniform (12 pts)	Kriging	0.0086	0.0180	0.0778
		RBF	0.0031	0.0065	0.0294
		GPR	0.0040	0.0085	0.0370
		Proposed	0.0007	0.0010	0.0029
	Non-uniform	Kriging	0.0390	0.0583	0.1702
		RBF	0.0052	0.0088	0.0245
		GPR	0.0084	0.0140	0.0388
		Proposed	0.0058	0.0092	0.0251
Ex2: $\sin(x)$ $x \in [0, 2\pi]$	Uniform (8 pts)	Kriging	0.0141	0.0206	0.0509
		RBF	0.0034	0.0052	0.0127
		GPR	0.0058	0.0088	0.0223
		Proposed	0.0007	0.0009	0.0022
	Non-uniform	Kriging	0.1240	0.2113	0.5141
		RBF	0.0338	0.0470	0.1031
		GPR	0.0878	0.1305	0.2992
		Proposed	0.0262	0.0366	0.0793

8 Conclusion

In this paper, we introduce a method for reconstructing curves based on a discrete version of the biharmonic equation. Our approach generates globally C^1 smooth curves that adapt naturally to various types of data and boundary conditions. It interpolates exact measurements while also enforcing inequality constraints, such as prescribed upper and lower bounds. Through experiments with both uniform and irregular data distributions, we found that the method consistently produces stable, oscillation free curves. This is particularly valuable in practical scenarios, where data are often sparse, noisy, or unevenly sampled. In addition, the method is flexible in handling both Dirichlet and Mixed boundary conditions.

Another significant strength lies in its physical interpretability: the biharmonic equation mimics the behavior of thin elastic beams or plates, providing an intuitive link between mathematical smoothness and physical phenomena.

Finally, the method naturally extends to higher dimensions, offering promise for applications such as surface reconstruction in geosciences, including bedrock topography estimation. Overall, this demonstrates the broader potential of the approach and opens pathways for future work, including integration of additional data sources and uncertainty quantification.

Acknowledgments

The authors would like to thank the Editor-in-Chief and the anonymous reviewers for their insightful comments and constructive suggestions, which significantly enhanced the clarity, rigor, and readability of this manuscript.

Conflict of Interest

The authors declare that they have no competing financial interests or personal relationships that could have influenced the work reported in this paper.

Funding

The authors did not receive any funding for this research.

References

Bastian, P., Blatt, M., Dedner, A., Dreier, N.-A., Engwer, C., Fritze, R., Gräser, C., Grüninger, C., Kempf, D., Klöfkorn, R., et al. (2021). The dune framework: Basic concepts and recent developments. *Computers & Mathematics with Applications*, *81*, 75–112.

Beirão da Veiga, L., Brezzi, F., Cangiani, A., Manzini, G., Marini, L. D., & Russo, A. (2013). Basic principles of virtual element methods. *Mathematical Models and Methods in Applied Sciences*, *23*(01), 199–214.

Bekele, S. S., Wolde, M. M., Führer, C., Kitterød, N.-O., & Kværnø, A. (2025). Modeling a smooth surface by a constrained biharmonic equation with application in soil science. https://arxiv.org/abs/2510.23195

Brezzi, F., & Marini, L. D. (2013). Virtual element methods for plate bending problems. *Computer Methods in Applied Mechanics and Engineering*, *253*, 455–462.

Chiles, J.-P., & Delfiner, P. (2012). *Geostatistics: Modeling spatial uncertainty*. John Wiley & Sons.

Cressie, N. (1993). *Statistics for spatial data*. Wiley.

de Boor, C. (2001). *A practical guide to splines* (3rd). Springer-Verlag.

Farin, G. (2002). *Curves and surfaces for cagd: A practical guide*. Morgan Kaufmann.

Gavin, H. P. (2014). Example of the principle of minimum total potential energy. *CEE 201L. Duke U*.

Hoffman, J. D., & Frankel, S. (2018). *Numerical methods for engineers and scientists*. CRC Press.

Journel, A. G., & Huijbregts, C. J. (1978). *Mining geostatistics*. Academic Press.

Kitterød, N.-O. (2017). Estimating unconsolidated sediment cover thickness by using the horizontal distance to a bedrock outcrop as secondary information. *Hydrology and Earth System Sciences*, *21*(8), 4195–4211.

Kitterød, N.-O., & Leblois, É. (2019). Modelling bedrock topography. *Earth Surface Dynamics Discussions*, 1–36.

Kitterød, N.-O., & Leblois, É. (2021). Estimation of sediment thickness by solving poisson's equation with bedrock outcrops as boundary conditions. *Hydrology Research*, *52*(3), 597–619.

Larson, M. G., & Bengzon, F. (2013). *The finite element method: Theory, implementation, and applications* (Vol. 10). Springer Science & Business Media.

Li, J., & Heap, A. D. (2008). A review of spatial interpolation methods for environmental scientists.

Mazarguil, A., Oudre, L., & Vayatis, N. (2022). Non-smooth interpolation of graph signals. *Signal processing*, *196*, 108480.

Ottosen, N., & Petersson, H. (1991, March). *Introduction to the finite element method* (2nd ed.). Division of Structural Mechanics, LTH.

Phillips, G. M. (2003). *Interpolation and approximation by polynomials* (Vol. 14). Springer Science & Business Media.

Piegl, L., & Tiller, W. (2012). *The nurbs book*. Springer Science & Business Media.

Quarteroni, A. (2009). *Numerical models for differential problems*. Springer.

Schumaker, L. L. (2007). *Spline functions: Basic theory* (3rd). Cambridge University Press.

Szilard, R. (2004). Theories and applications of plate analysis: Classical, numerical and engineering methods. *Appl. Mech. Rev.*, *57*(6), B32–B33.

Xu, Y., & Xu, R. (2022). Research on interpolation and data fitting: Basis and applications. *arXiv preprint arXiv:2208.11825*.

Zarowski, C. J. (2004). *An introduction to numerical analysis for electrical and computer engineers*. John Wiley & Sons.